RAA 2021 Vol. **21** No. **6**, 142(13pp) doi:10.1088/1674-4527/21/6/142

http://www.raa-journal.org *http://iopscience.iop.org/raa*

Research in Astronomy and Astrophysics

Stellar activity cycles as revealed by long-term beat-like patterns from light curves of *Kepler*

Heng-Geng Han[1,2], Kai-Ming Cui[1,2], Ji-Feng Liu[1,2,3], Hui-Qin Yang[1], Xuan Fang[1,4] and Rui-Ning Zhao[1,2]

[1] CAS Key Laboratory of Optical Astronomy, National Astronomical Observatories, Chinese Academy of Sciences, Beijing 100101, China; *hghan@nao.cas.cn*

[2] School of Astronomy and Space Sciences, University of Chinese Academy of Sciences, Beijing 100049, China

[3] WHU-NAOC Joint Center for Astronomy, Wuhan University, Wuhan 430072, China

[4] Department of Physics & Laboratory for Space Research, Faculty of Science, the University of Hong Kong, Hong Kong, China

Received 2020 December 10; accepted 2021 February 5

Abstract Stellar activity cycles have been found on many stars through different methods. Although in debate, an empirical relation has been found where a period of stellar activity cycle $P_{\rm cyc}$ is positively correlated with rotation period $P_{\rm rot}$ along some segregated branches. In this work, we built a systematic process to search for the *Kepler* objects that are analogous to the long-term solar brightness variations and investigate their possible origins. After a rigorous selection, we obtained 43 objects that all exhibit clear long-term beat-like patterns and their variability (amplitude of rotational modulation) periods and rotation periods were derived. Due to the 4-year duration of the *Kepler* mission, our targets are located in the region where the cycle periods are longer than ∼1 yr and shorter than ∼2.5 yr. However, all of our targets exhibit clear and notable quasi-periodic variations in variability, yet we cannot confirm any linear trends that were predicted by previous research independently. This may suggest that in the *Kepler* realm of the $P_{\rm cyc}$–$P_{\rm rot}$ diagram, these relations would mix with each other or the beat-like patterns may not be related to the stellar cycle unless other evidence is provided.

Key words: stars: activity — starspots — stars: rotation

1 INTRODUCTION

Stars with convective envelopes could develop magnetic fields according to the dynamo theory (e.g. Parker 1955a; Charbonneau 2010). Magnetic fields would float up to the photospheres when the magnetic buoyancy is large enough (Parker 1955b; Solanki et al. 2006), forming the active regions, which manifest as dark spots and bright faculae. The number of sunspots has an 11 yr period (e.g. Schwabe 1843; Harvey 1992), known as solar cycle, which reflects the long-term variation of the solar magnetic fields as detected through the Zeeman effect (Babcock 1953). The strength of chromospheric activity can be characterized by the line core emission of Ca II H&K (e.g. Babcock & Babcock 1955; Leighton 1959), which are good indicators of magnetic activity level. The S-index, calculated from the emission of Ca II H&K lines, also exhibit cyclic variation during a solar cycle (Egeland et al. 2017).

Inspired by the Sun, Wilson (1978) found periodic changes in the stellar Ca II H&K emission lines through a monitoring program at the Mount Wilson Observatory (MWO). This periodic behavior of magnetic fields on stars other than the Sun has been extensively discussed since then. Brandenburg et al. (1998) and Saar & Brandenburg (1999) analysed the data from MWO and found two branches of stars, i.e., the active one (A branch) and the inactive one (I branch). Moreover, the lengths of magnetic activity cycles $P_{\rm cyc}$ were observed to be proportional to rotation periods $P_{\rm rot}$ on each branch and these branches could also exist in other stellar types (Böhm-Vitense 2007). Recently, Metcalfe et al. (2016) reappraised this correlation by adding the *Kepler* asteroseismic targets as well as data from previous literature (Hall et al. 2007; Metcalfe et al. 2010, 2013; Egeland et al. 2015) and found similar results.

Besides chromospheric activities, brightness variations can also be used as tracers of a magnetic activity level. Solar brightness variations are dominated by different magnetic components on different timescales. Typically, faculae are dominant on timescale over the solar cycle while sunspots are dominant on rotational timescale (Shapiro et al. 2016, 2017). Along with the solar cycles, the

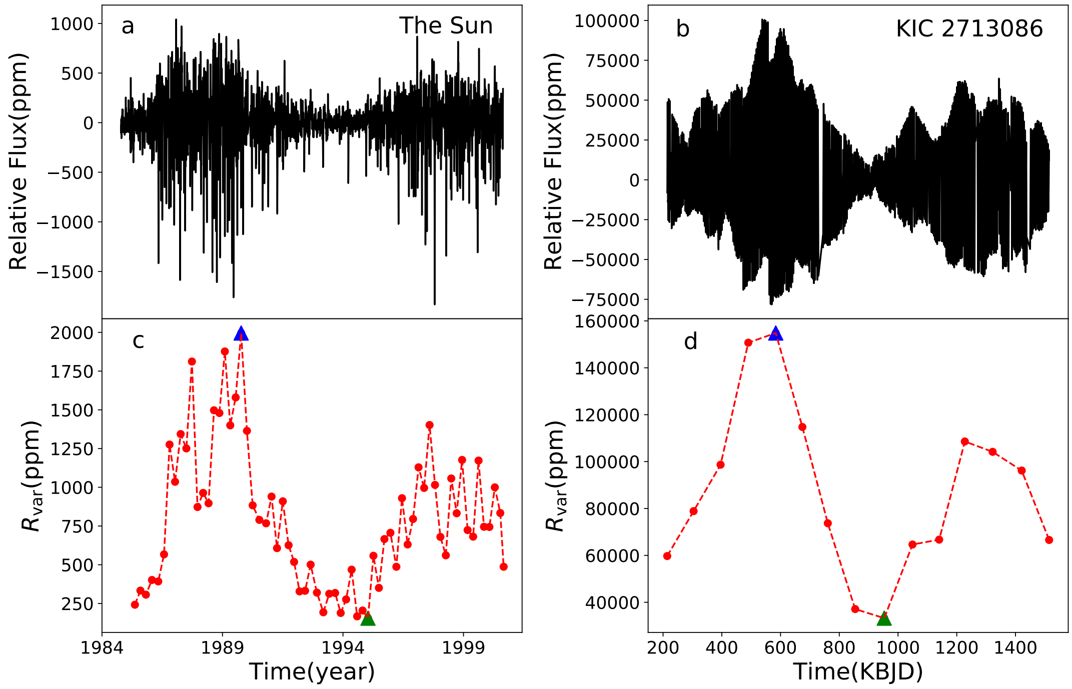

Fig. 1 Panel (a): The Solar LC with daily cadence. Panel (b): LC of KIC 2713086 with 30-min cadence. Panel (c): $R_{\rm var}$ curve of Solar LC. Panel (d): $R_{\rm var}$ curve of LC of KIC 2713086. Maxima and minima $R_{\rm var}$ curves are marked by blue and green triangles, respectively. KBJD is the *Kepler* Barycentric Julian Day, which is a Julian day minus 2454833.0 (UTC = 2009 January 1 12:00:00) and correlated to the arrival times at the barycenter of the Solar system.

total solar irradiance shows quasi-periodic variations (e.g. Solanki et al. 2013; Shapiro et al. 2016) and it is in-phase with the variations of solar S-index (e.g. Preminger et al. 2011). Meanwhile, solar light curves also exhibit changes in variability (amplitude of rotational modulation) during solar cycles (Shapiro et al. 2016; Salabert et al. 2017), which are caused by the evolution of sunspots.

Similar phenomena have been observed on other stars. Long-term brightness variations of stars may be correlated to cyclic variations of chromospheric activities, either in phase or in anti-phase (Reinhold et al. 2019). Young stars are spot-dominated and they would be less luminous during chromospheric activity maxima while old stars are faculae-dominated and they would become brighter during activity maxima (Radick et al. 1998). Recently, the *CoRoT* and the *Kepler* spacecraft have observed lots of light curves (hereafter LCs) with modulation on rotational timescales. Similar to the Sun, such modulation may be dominated by starspots and thus their amplitudes can be used as a good proxy of stellar activity (e.g. Maehara et al. 2017; Yang et al. 2017; Reinhold et al. 2020).

More and more literature is focusing on searching for activity cycles through photometric analysis. Based on time-frequency analysis, some literature studied the periodic variations of frequencies of LCs, which indicate possible stellar cycles (Oláh et al. 2009; Vida et al. 2014; Mathur et al. 2014). Through analyzing variability changes, Ferreira Lopes et al. (2015) proposed a new sequence besides active and inactive sequences named "short-cycle branch". Recently, Montet et al. (2017) recovered the long-term brightness variations from the Kepler full-frame images and found some targets exhibit cyclic brightness variations. McQuillan et al. (2014) provided an ideal sample for studying stellar activity cycles, which contains rotation periods of 34 030 *Kepler* targets. Based on this sample, Reinhold et al. (2017) found possible magnetic cycles of 3203 targets.

Variability of solar light curves changes during a solar cycle (Shapiro et al. 2016; Salabert et al. 2017), which looks like beat patterns. In this work, we built a systematic process to search for *Kepler* targets whose LCs exhibit the long-term beat-like patterns, which are similar to the variability on solar LCs, and investigate their possible origins. Such elite samples would be useful for understanding stellar evolution, stellar activity and stellar dynamo.

2 TARGET SELECTION AND DATA ANALYSIS

2.1 The Kepler Data

In 2009 NASA launched the *Kepler* spacecraft to mainly search for exoplanets (Koch et al. 2010). *Kepler* has a 0.95m-diameter aperture and a 115.6 square degrees field of view. It has a high photometric precision of 10 ppm for bright targets (V band magnitude is 9–10) and 100 ppm for faint targets (V band magnitude is 13–14). Two kinds

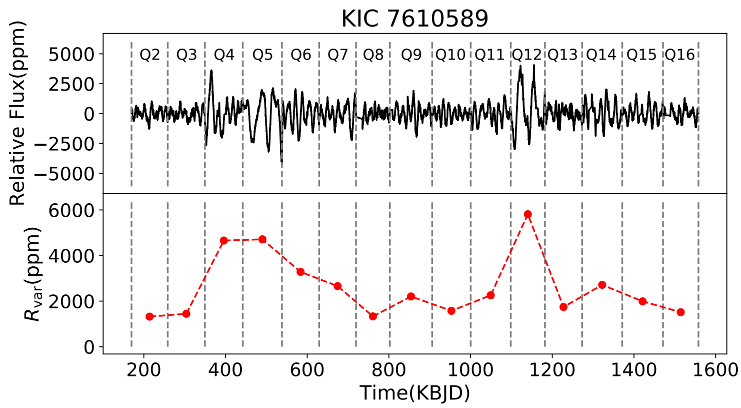

Fig. 2 Example of the target that shows abrupt change in variability. Quarter names are marked, which keep the same to other figures shown in this paper. It is clear that the variability suddenly changes at Q12. Targets like this are not included in the final list.

of data with different time resolutions are provided: one is long-cadence data with a 30 min sampling time interval; the other is short-cadence data with a 1 min sampling time interval. Only about 5000 targets have short-cadence data and the observing time is relatively short, thus we used long-cadence data in this work. Two kinds of LCs, named SAP and PDC LCs, were derived based on the Kepler data pipelines (Van Cleve & Caldwell 2016). We simply focused on the variability of LCs so that we chose to use PDC LCs from *Kepler* mission archive (DR 25)[1]. Meanwhile, SAP LCs were also used for inspection.

2.2 Targets Selection and Detection Method

Variability of solar LCs changes during solar cycles. Amplitudes are large during activity maximum and small during activity minimum (Yeo et al. 2014; Shapiro et al. 2016; Salabert et al. 2017), which forms a long-term beat-like pattern. In panel (a) of Figure 1, the solar LC is shown. We used the composite total solar irradiance data from Fröhlich & Lean (1998). Similar to the *Kepler* data, the solar data were divided into bins with a 90-day length, i.e., a quarter length of *Kepler* data. Then for the LC in each bin the linear trend was removed and we calculated the relative flux in each bin. Not only the Sun, we noticed that some LCs of *Kepler* targets also exhibit similar patterns. In panel (b) of Figure 1 we gave a typical example, KIC 2713086. Its LC also exhibited clear long-term quasi-periodic amplitude variations.

In order to find *Kepler* targets with such a shape of LCs and quantify the long-term quasi-periodic amplitude variations, the well-known $R_{\rm var}$ was calculated. Following the definition given in previous literature (e.g. Basri et al. 2011), we defined the variability $R_{\rm var}$ as the difference between 5th and 95th of relative flux of each quarter. The midpoint of observing time of each quarter was used to denote time of each $R_{\rm var}$ point. Then for each target a $R_{\rm var}$ curve was derived, which can be used to quantify the amplitude variations. For example, in Figure 1 red dashed lines with dots represent the $R_{\rm var}$ curves and corresponding $R_{\rm var}$ of each quarter. Noticing that, all the LCs analysed in this work were smoothed through a 10 h length window to exclude extreme outliers, noises and most flares.

During stellar activity cycles, brightness variations are dominated by starspots and faculae (Shapiro et al. 2016, 2017). As a result, we mainly focused on targets that exhibit rotational modulation and it is necessary to avoid possible contaminations. First, LCs of eclipsing binaries (EBs) are sometimes similar to those of stars with starspots (Balona 2013), making it difficult to distinguish them. Second, among the main-sequence stars there are some kinds of pulsating stars. They pulsate in different modes driven by different mechanisms (e.g. Breger 1979; Dziembowski et al. 1993; Kaye et al. 1999). If the pulsators develop multiple adjacent pulsating frequencies, their LCs could show beat phenomena in variability. Therefore, in this work, we used the catalog provided by McQuillan et al. (2014), in which possible pulsators and EBs were excluded.

Not all the targets have been consecutively observed for 4 yr. Many targets exhibit break quarters with no observing data, which makes it difficult to get the reliable $R_{\rm var}$ curve of long-term beat-like patterns. Thus we need to drop targets with short observing time. Considering that observing time of Quarter 0, Quarter 1 and Quarter 17 are relatively short, we excluded these three quarters before the data processing. Then we calculated the number of observation quarters of all the targets. After that, we dropped targets with less than 14 observation quarters and 24 517 targets left, roughly 73 percent of the data.

As is shown in Figure 1, the amplitudes of the solar LC varies significantly between solar minimum and solar maximum. In order to find more targets with notable amplitude variations in the *Kepler*, we defined a ratio

[1] *http://archive.stsci.edu/kepler*

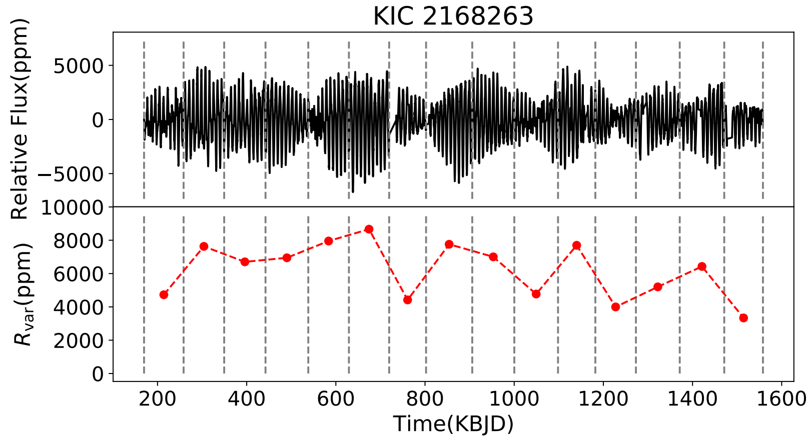

Fig. 3 Example of a target whose $R_{\rm var}$ curve shows short-term variations during the observation. This kind of target is not included in the final list.

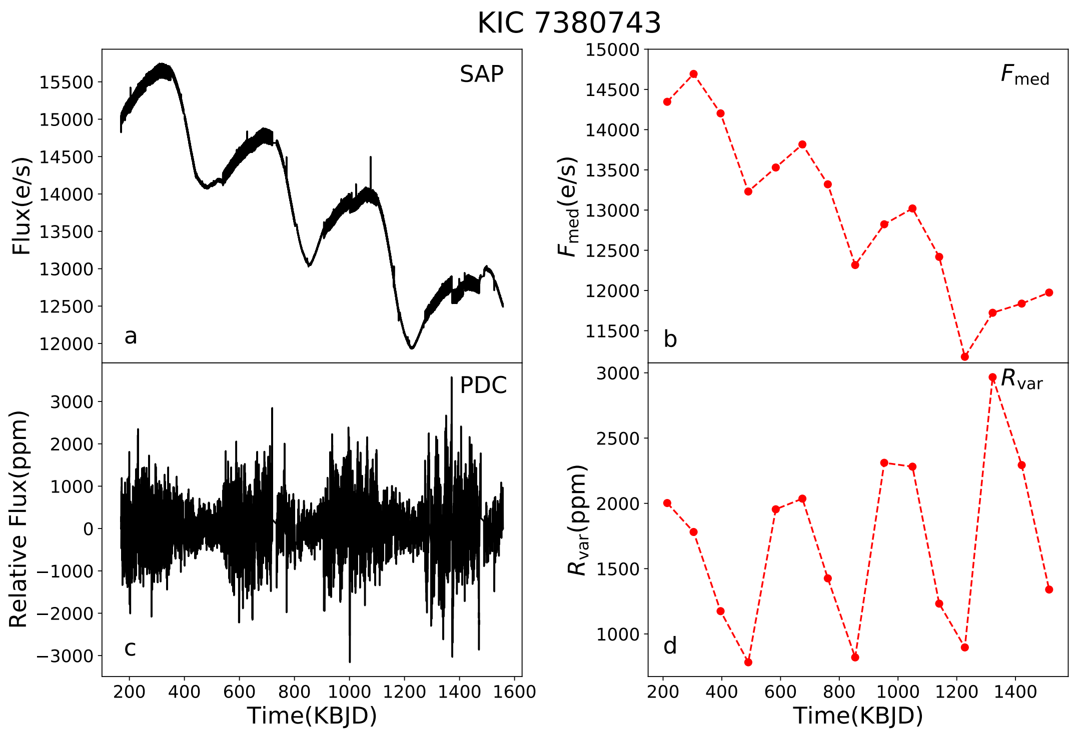

Fig. 4 Comparison between SAP LC and PDC LC of KIC 7380743. The SAP LC is concatenated and shifted to keep the median value unchanged compared to the raw SAP LC. It is obvious that amplitude variation of PDC LC is in-phase with the one-year modulation shown in SAP LC. In panel (b) the $F_{\rm med}$ curve is shown and in panel (d) the $R_{\rm var}$ curve is shown. The $F_{\rm med}$ curve is a sequence which is the combination of median flux and the middle time of each quarter of the SAP LC. It is clear that the $R_{\rm var}$ curve is also in-phase with the $F_{\rm med}$ curve. Such a kind of target is not included in our final sample.

of minimum $R_{\rm var}$ to the maximum $R_{\rm var}$ for each $R_{\rm var}$ curve, i.e., $q = \min\{R_{\rm var}\}/\max\{R_{\rm var}\}$. For instance, the $\min\{R_{\rm var}\}$ and $\max\{R_{\rm var}\}$ are indicated in the $R_{\rm var}$ curves of Figure 1. Therefore, q is a quantity less than 1 and the smaller the q is, the greater the variation of amplitude would be. Then, we calculated the mean value $\overline{q}$ for our sample and dropped stars with $q > \overline{q}$. After this step, 13 373 targets remained.

Meanwhile, we noticed that the variability of the Sun changes slowly during a solar cycle. Thus, for each target, if a $R_{\rm var}$ value changes significantly than its adjacent quarters, it should be dropped. For example, Figure 2 shows an object with a sudden variation in Q12 in its $R_{\rm var}$ curve. This phenomenon could be physical or systemic. Some transients or outbursts may lead to their $R_{\rm var}$ change rapidly, and the PDC procedure would also under-subtract or over-subtract some signals (e.g. Stumpe et al. 2012; Van Cleve & Caldwell 2016; Cui et al. 2019). Therefore, for each quarter of every target, we calculated the ratio of $R_{\rm var}$ for the two quarters before and after. To make use of our previous mean ratio $\overline{q}$, we always calculated the ratio of the smaller $R_{\rm var}$ to the larger $R_{\rm var}$. If a quarter has a ratio less than $\overline{q}$, we considered that there is an abrupt change in variability and this object should be dropped. After this step, we have 8001 targets left.

In addition to such scenario, in order to find targets with long-term amplitude variations, the $R_{\rm var}$ curves should not vary frequently. Thus in our work, the total number of maxima and minima points is limited to be less than 8. Since our targets have 14 quarters at least, the period of a $R_{\rm var}$ curve is at least $\sim$1 yr. Figure 3 shows an example with rapid variations. After all these selection steps mentioned above, we have 5363 targets left.

Even so, the amplitude variations may still be due to other non-physical causes. The most notable case is the orbital motion of the *Kepler*. The *Kepler* orbital period and the Earth orbital period are almost the same (Van Cleve & Caldwell 2016). We noticed that many SAP LCs exhibit clear modulation related to the orbital motion, causing the LC to show nearly one-year period. Meanwhile, some PDC LCs exhibit amplitude variations that are associated with this one-year signal. Such modulation shown in SAP LCs may affect the PDC LCs. Figure 4 shows a typical example, after we checked its target pixel file, we found the aperture size varies with the satellite's orbital period, causing a one-year variation on its LC and $R_{\rm var}$ curve.

Considering that SAP reserves the systematic trends caused by satellite motion, we used a simple method to exclude these contaminations with checking their corresponding SAP LCs. First, we stitched all the quarters of SAP LCs end to end to create the combined SAP LCs and kept the median flux unchanged compared to the raw SAP LCs. Then we calculated the median flux in each quarter. Combining the median flux with the middle time of each quarter, we got a $F_{\rm med}$ curve, which reflects the long-term trends of SAP LCs (see Fig. 4 in detail). After that, both the $R_{\rm var}$ and $F_{\rm med}$ curves were normalized and the cross-correlation function was applied to check whether they are in-phase with each other. The larger the absolute value of the cross-correlation function, the more likely that the two curves are in-phase. The proper threshold of cross-correlation function was decided through trail and error with visual checking. Finally the absolute value of cross-correlation function was chosen to be 9. Targets with absolute value of cross-correlation function larger than 9 were dropped and there are 4707 targets left.

Now we derived a relatively small sample and we began to search for targets whose LCs exhibit amplitude variations that are similar to the solar LCs through visual inspection. Yang & Liu (2019) built a working platform named *The Kepler Data Integration Platform*[2], which integrates many aspects of data analysis on the whole *Kepler* dataset, including pictures of all the LCs that can be zoomed in or out dynamically. The efficiency of visual inspection has been greatly improved by the working platform. During the inspection, most of our targets do not exhibit long-term beat-like patterns. They mainly have such characteristics:

1. First, it is common that the $R_{\rm var}$ curves do not exhibit any periodic behavior though the variability changes significantly. In panel (a) of Figure 5 we gave an example: KIC 1295289. The $R_{\rm var}$ curve does not exhibit any clear period. This kind of targets can be

Table 1 Stellar parameters of targets analysed in this work. Rotation periods are from McQuillan et al. (2014). $T_{\rm eff}$ and $\log g$ are from KIC (Brown et al. 2011). Targets that are also in Reinhold et al. (2017) sample are marked by asterisks.

KIC ID	$P_{\rm rot}$ (d)	$T_{\rm eff}$ (K)	$\log g$ (Dex)	$P_{\rm beat}$ (yr)
2713086	4.140	3920	4.700	2.17
3539331	1.541	4338	4.618	1.23
3539475	25.996	4677	4.633	1.95
3544959*	15.447	5345	4.571	2.25
3648913*	10.771	5721	4.224	2.41
3748172	1.054	3994	4.701	2.05
4819507*	17.015	5675	4.100	1.97
5623589*	23.806	5263	4.565	2.05
5779298*	17.944	5126	4.586	2.08
5795551*	11.825	4685	4.592	1.62
5965087*	11.756	6116	4.487	2.52
6301466*	15.217	5208	4.606	1.73
6386695	13.597	5574	4.532	2.03
6525409	12.385	5452	4.572	1.59
6591498	12.427	5325	4.484	1.84
6763859	19.596	4602	4.559	1.53
6848592	1.653	5670	4.434	1.15
6949412	1.647	3666	4.797	2.25
6955009*	17.911	4891	4.583	2.03
7031066*	18.712	5115	4.439	1.45
7038460*	10.770	5726	4.476	1.48
7186846*	13.217	6004	4.484	2.55
7816203	1.610	5452	4.487	1.84
7943846*	22.360	5043	4.473	1.89
8249139*	10.485	5395	3.779	1.78
8415004	1.230	3731	4.742	1.78
8689739*	25.652	5092	4.376	1.81
8776565	2.681	3502	4.925	1.62
9574706	28.053	3940	4.726	2.05
9592939*	11.181	4987	4.611	1.48
9639021*	11.944	5349	4.478	1.83
10056447*	6.687	5815	4.547	1.78
10082542*	11.318	4987	4.604	1.78
10598045*	18.045	4944	3.965	1.51
10711756	7.560	5300	4.033	1.29
10905040	33.558	5126	4.578	1.97
11463171	21.547	5513	4.534	1.12
11673463	12.507	6036	4.029	1.92
11764306*	25.375	4530	4.617	2.30
11874061*	21.292	4864	4.595	1.51
12067439*	15.890	4846	4.569	0.96
12216258*	18.721	5062	4.610	1.78
12315104*	9.329	5314	4.562	1.48

[2] http://kepler.bao.ac.cn

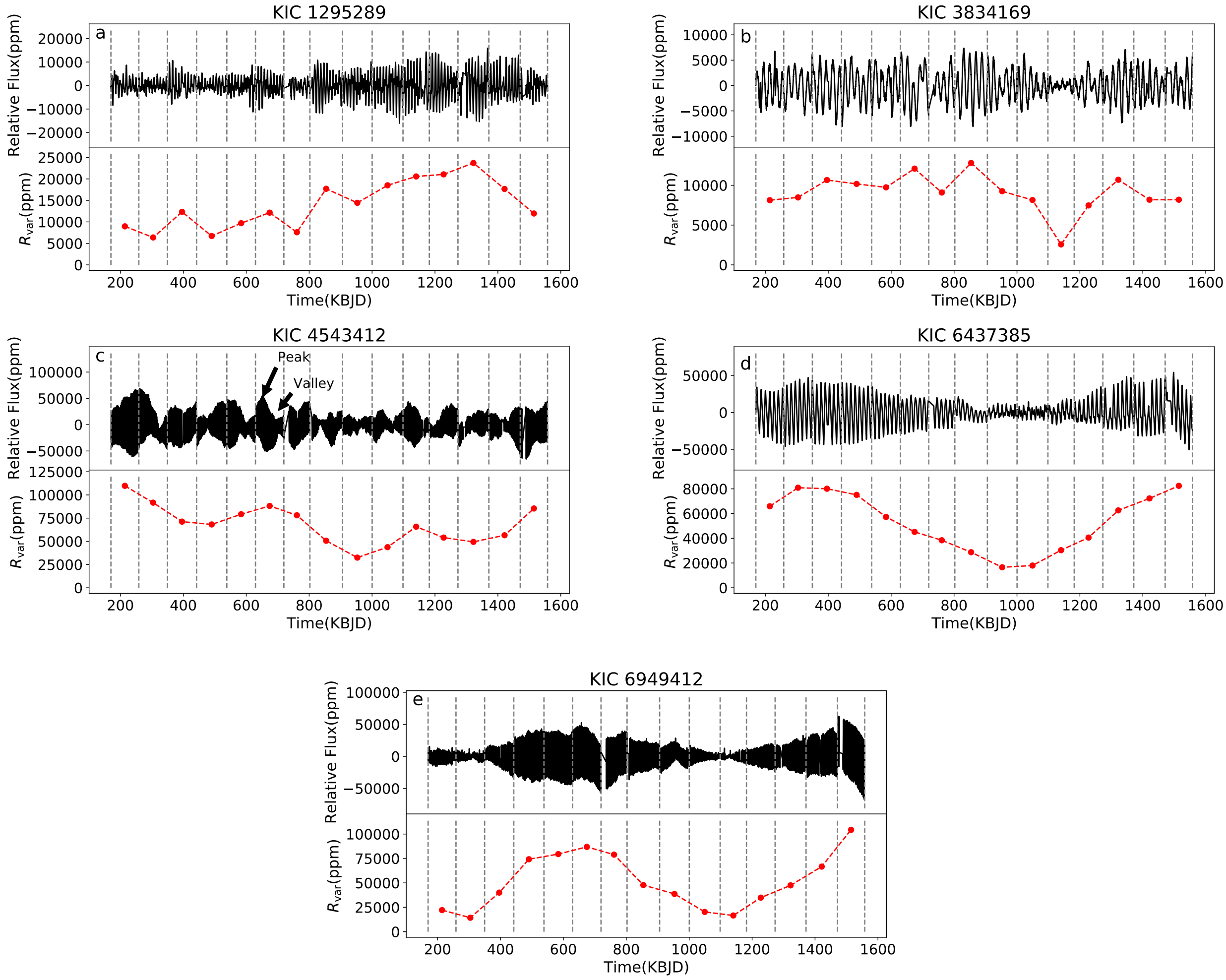

Fig. 5 Typical examples of different kinds of situations that should be treated separately. Panel (a): a target with no clear variability period. Panel (b): a target whose amplitudes of LC did not change significantly after the minimum appears. Panel (c): a target whose variability changes quickly, causing one single quarter exhibits both maximum and minimum. Panel (d): a target that exhibits an $R_{\rm var}$ period longer than 4 yr. Panel (e): a target with a certain maximum of an $R_{\rm var}$ curve that locates at the last quarter. In the final list, KIC 6949412 is kept.

easily identified when we looked through the LCs. As a result, we managed to drop these targets simply through visual inspection.

2. Variability of a LC may not change significantly after it reaches the maxima or minima. In such case it is difficult to decide the true $R_{\rm var}$ period. From panel (b) of Figure 5 we can find that the $R_{\rm var}$ curve only shows one relatively small value in one certain quarter. However, the $R_{\rm var}$ value does not change significantly in other quarters. Those targets do not exhibit regular $R_{\rm var}$ variations. We mainly focused on quasi-periodic amplitude variations, so that this kind of targets was also dropped.
3. Sometimes amplitudes of LCs could change very quickly. In a single quarter, the amplitudes may have a peak and a valley (see panel (c) of Fig. 5 as an example). However, we only used one specific value $R_{\rm var}$ to quantify the variability of LC in one quarter. In such case, from the $R_{\rm var}$ curve we cannot get the valid period of $R_{\rm var}$ curve, since our $R_{\rm var}$ curves are only suitable for finding long-term variations. Targets with such a character were also dropped during the visual inspection process.
4. Observation time of *Kepler* is roughly 4 yr so that period of the $R_{\rm var}$ curve longer than or close to 4 yr cannot be detected. Through visual inspection we found that for some targets the $R_{\rm var}$ curve periods are longer than 4 yr, which makes the $R_{\rm var}$ curve only show part of the whole $R_{\rm var}$ curve. KIC 6437385 is a typical example, which was shown in panel (d) of Figure 5. This kind of targets was dropped because their periods could be underestimated.
5. Since we mainly focused on long-term variations shown in $R_{\rm var}$ curves, it is likely that some of the

maxima or minima locate at the beginning or the end of $R_{\rm var}$ curves. This would lead to difficulties in deciding whether these maxima or minima are valid. For example, from the $R_{\rm var}$ curve of KIC 6949412 (panel (e) of Fig. 5) we can clearly find quasi-periodic variation but the second maximum appears in the last quarter. However, the shape of the $R_{\rm var}$ curve is quite symmetric. As a result, for this kind of targets, even though the maxima or minima may locate at the beginning or the end of the $R_{\rm var}$ curve, we still kept them.

3 RESULTS

After the final selection process, we had 43 targets left and their LCs together with $R_{\rm var}$ curves are shown in Appendix A. To ensure the reliability of our results, we also checked their pixel data and obtained similar light curves after changing to larger apertures. Considering that these beat-like patterns may be associated with the possible activity cycles, we first calculated their periods.

It is common to use the *Lomb-Scargle* periodigram (Lomb 1976; Scargle 1982) to detect period of a dataset. However, it assumes a strictly periodic scenario, which is generally not the case in stellar activity cycles. In addition, the length of solar cycle varies from 8 to 11 yr. It is more appropriate to use a quasi-periodic model to detect the cycle period (Olspert et al. 2018). Combining with the maxima and minima of $R_{\rm var}$ curves and the actual shape of LCs, we manually calculated the periods of long-term beat-like patterns according to visual inspection and for each target the period is defined to be the time interval between the vertical pink lines shown in Appendix A. One target might exhibit multiple periods and we used their mean as the activity cycle length because the periods do not vary significantly.

The final results together with the stellar parameters are listed in Table 1. All these 43 targets exhibit clear beat-like patterns, which may be associated with underlying activity cycles. 25 objects of our sample are also in the sample of Reinhold et al. (2017) and they are marked by asterisks in Table 1. Our work concentrates on photometric analyses and there are three main differences between this work and Reinhold et al. (2017). (1) All of our targets exhibit notable amplitude variations that are similar with those shown in solar LCs. (2) We built a systematic process to exclude possible contaminations. (3) Our period detection was based on the manual inspection because of the quasi-periodic variations of $R_{\rm var}$ curves.

4 DISCUSSION AND CONCLUSIONS

The empirical relations between cycle period ($P_{\rm cyc}$) and rotation period ($P_{\rm rot}$) have been extensively discussed (e.g. Saar & Brandenburg 1999; Böhm-Vitense 2007; Metcalfe et al. 2016). According to their chromospheric activity levels, stars can be divided into two sequences, i.e., the "Active-branch" ("A-branch") and the "Inactive-branch" ("I-branch") (e.g. Saar & Brandenburg 1999; Böhm-Vitense 2007). After the *CoRoT* and the *Kepler* spacecrafts were launched, much attention was drawn to searching activity cycles based on photometric data (e.g. Ferreira Lopes et al. 2015; Reinhold et al. 2017). Ferreira Lopes et al. (2015) discovered activity cycles of 16 *CoRoT* targets by analyzing the photometric data. Their results showed that besides the "A" and "I" branches, a third branch may exist, called the "short-cycle" branch ("s-branch").

Considering that the long-term beat-like patterns may be related to activity cycles, we present our targets in Figure 6 along with the data from previous literature (Saar & Brandenburg 1999; Böhm-Vitense 2007; Hall et al. 2007; Metcalfe et al. 2010, 2013; Egeland et al. 2015; Ferreira Lopes et al. 2015; Metcalfe et al. 2016). In the right panel of Figure 6, we give a zoom-in for the *Kepler* duration region. Different lines in Figure 6 represent different branches given by previous works (Böhm-Vitense 2007; Ferreira Lopes et al. 2015; Metcalfe et al. 2016). Filled circles represent our targets and different colours stand for different effective temperatures. Due to the limitation of *Kepler* duration, our targets concentrate in the area where $P_{\rm cyc}$ is larger than ∼1 yr and smaller than ∼2.5 yr. As a result, our targets are located in the lower extrapolation region of the $P_{\rm cyc}$–$P_{\rm rot}$ relations.

Some fast rotating stars with $P_{\rm rot}$ shorter than 5 days are close to the "A-branch". Since the number of our targets is limited, near the "A-branch" there is no clear cluster of stars. Moreover, some previous literature also questioned the "A-branch". Olspert et al. (2018) found a cluster of active stars but the linear trend was not confirmed. Boro Saikia et al. (2018) also questioned the existence of "A-branch" given by both Saar & Brandenburg (1999) and Böhm-Vitense (2007). Usually, "A-branch" stars exhibit higher chromospheric activity level compared to "I-branch" stars. Higher chromospheric activity indicates a stronger magnetic field level. Magnetic fields are maintained by the stellar dynamo, which depends on the depth of the convection envelope (Parker 1955a; Noyes et al. 1984; Wright et al. 2011). As a result, "A-branch" stars might tend to have lower effective temperature compared to "I-branch" stars. Although our sample is small, stars in this region tend to exhibit lower effective temperatures. This may be a possible indication of the "A-branch". However, due to the lack of clear evidence, the existence of "A-branch" is still doubtable.

Unlike the "A-branch", the "I-branch" has been confirmed by varies literature. For example, although Olspert et al. (2018) and Boro Saikia et al. (2018) questioned the "A-branch", their results still supported the existence of "I-branch". $P_{\rm cyc}$–$P_{\rm rot}$ relations shown in the diagram of Reinhold et al. (2017) is weak but along the "I-branch" there are more targets compared to other regions.

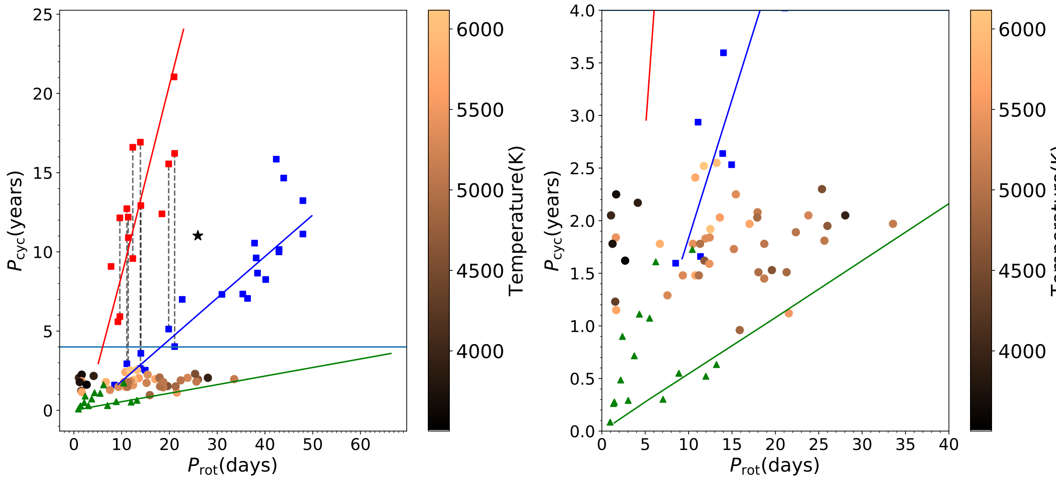

Fig. 6 $P_{\rm cyc} - P_{\rm rot}$ plane given by Metcalfe et al. (2016), which also includes data from previous literature. Squares are data from Saar & Brandenburg (1999); Böhm-Vitense (2007); Hall et al. (2007); Metcalfe et al. (2010, 2013); Egeland et al. (2015); Metcalfe et al. (2016) and triangles are data from Ferreira Lopes et al. (2015). The Sun is denoted by the star mark. Dashed vertical lines connect two different cycles detected on one target. Blue horizontal line is the duration of *Kepler*. Filled circles are our targets and different colours stand for different effective temperatures. Different lines represent different branches. Right panel: a zoom-in for the *Kepler* duration region.

Meanwhile, many of our targets are close to the "I-branch" and some of them clearly match this sequence. However, similar to the result of Reinhold et al. (2017), our results also show large dispersion in this region. Furthermore, in the $P_{\rm cyc}$–$P_{\rm rot}$ diagram of Reinhold et al. (2017) there are also more targets lying in the region between the "I-branch" and "s-branch". From Figure 6 it is easy to find that some of our targets also lie in this region. As a result, due to the large dispersion of our data, though many targets are close to the "I-branch", no linear trend of $P_{\rm cyc}$–$P_{\rm rot}$ relation can be confirmed simply based on our results.

As for the "s-branch" proposed by Ferreira Lopes et al. (2015), although the *Kepler* has longer duration compared to the *CoRoT*, we only have three targets that lie on this "s-branch". There are more targets located in the region between the "I-branch" and the "s-branch". Considering that the "s-branch" is an empirical relation based on few data points, we suggested that this branch may not be physical.

Although after a rigorous selection based on the prior characteristics of the solar LCs we got an elite sample of *Kepler* targets that all exhibit clear long-term beat-like patterns, we still cannot confirm the existence of these three $P_{\rm cyc}$–$P_{\rm rot}$ relations. There may be some possible interpretations. (a) Because of the limited duration of the *Kepler*, we can only detect one or two cycles for each target. This may lead to large uncertainties in the cycle periods. (b) Böhm-Vitense (2007) suggested that on different branches, the dynamos are different and they operate in different layers of stars. This leads to different dependence of $P_{\rm cyc}$ on $P_{\rm rot}$. Maybe in the narrow *Kepler* region of the $P_{\rm cyc}$–$P_{\rm rot}$ diagram, these different dynamos generate stellar activity cycles that are identical. As a result these three sequences finally mix with each other. (c) The $P_{\rm cyc}$–$P_{\rm rot}$ relations are derived based on chromospheric proxies. It could be different for photometric proxies (e.g. Distefano et al. 2017). It is possible that the beat-like patterns shown in the LCs are not related to the stellar cycles unless some other evidence is provided.

In fact, the modulation of amplitude is a complex scenario, which may be related to many aspects, including the position, size and number of starspots (Basri 2018; Basri & Shah 2020). Recently, Basri & Shah (2020) argued that the changes in starspots asymmetries, i.e., the distribution of starspots, instead of the coverage, could mainly attribute to the changes in the LC variability. The amplitude of LC could reflect the asymmetries of starspot distribution. Meanwhile, differential rotation also plays an important role in the LC variability. In general, there is a large degeneracy in all these starspot parameters while analyzing the LC variability. It is very difficult to determine what is the main contributor. Further long-term photometric and spectroscopic observations are required to break such large degeneracy. Nevertheless, in this work we provided an elite sample of stars that all exhibit long-term beat-like patterns in their LCs. Such samples would be useful for further research in stellar activity and stellar dynamos.

Appendix A: LCS AND $R_{\rm VAR}$ CURVES

We showed all the LCs of our targets together with the $R_{\rm var}$ curves in this section. The pink lines denote the times that were used to calculate the activity cycle periods in this work.

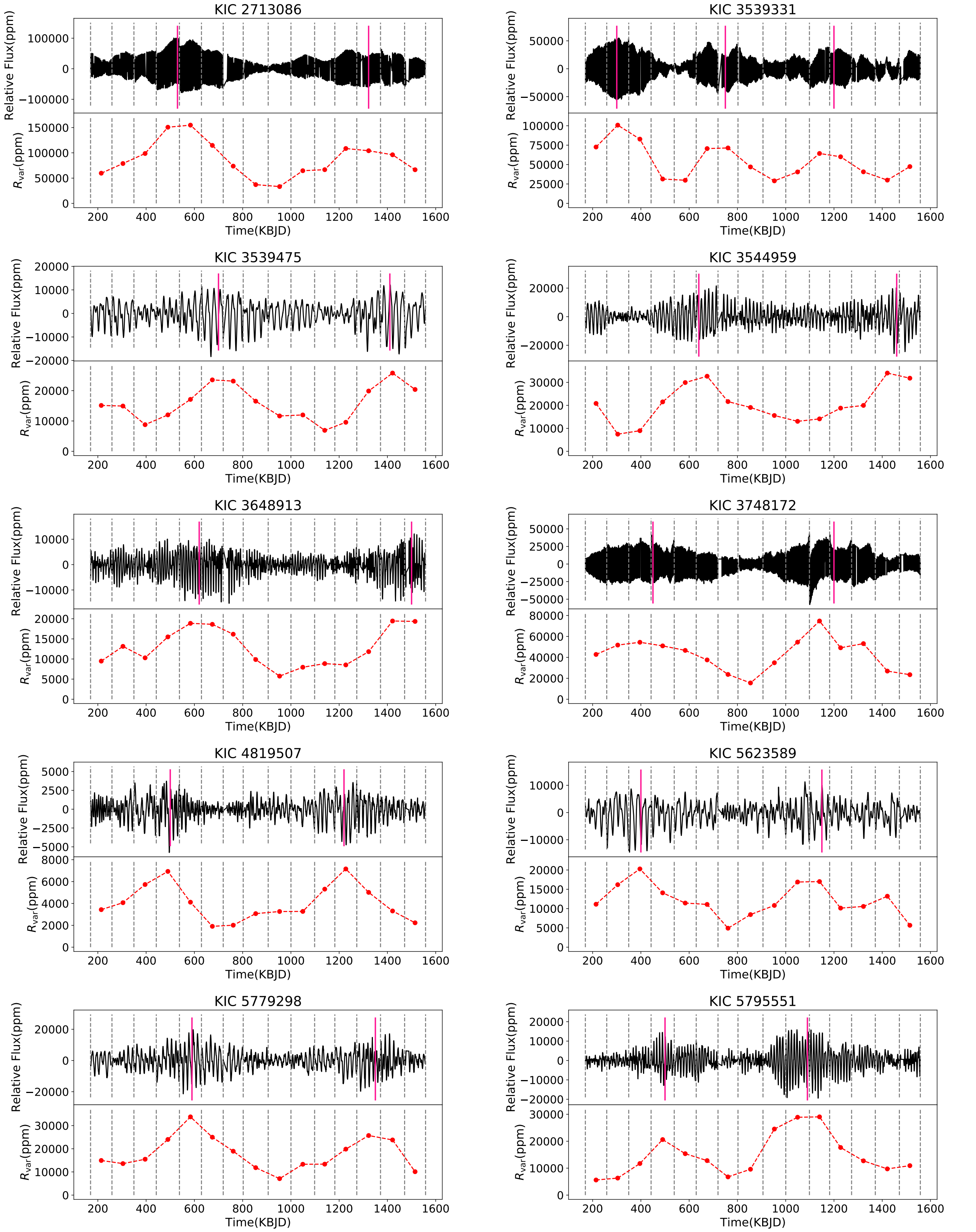

Acknowledgements This work is supported by the Strategic Priority Research Program of Chinese Academy of Sciences (Grant No. XDB 41000000). Jifeng Liu acknowledges the support from the National Natural Science Foundation of China (NSFC, Grant Nos. 11988101 and 113300034) and the National Key

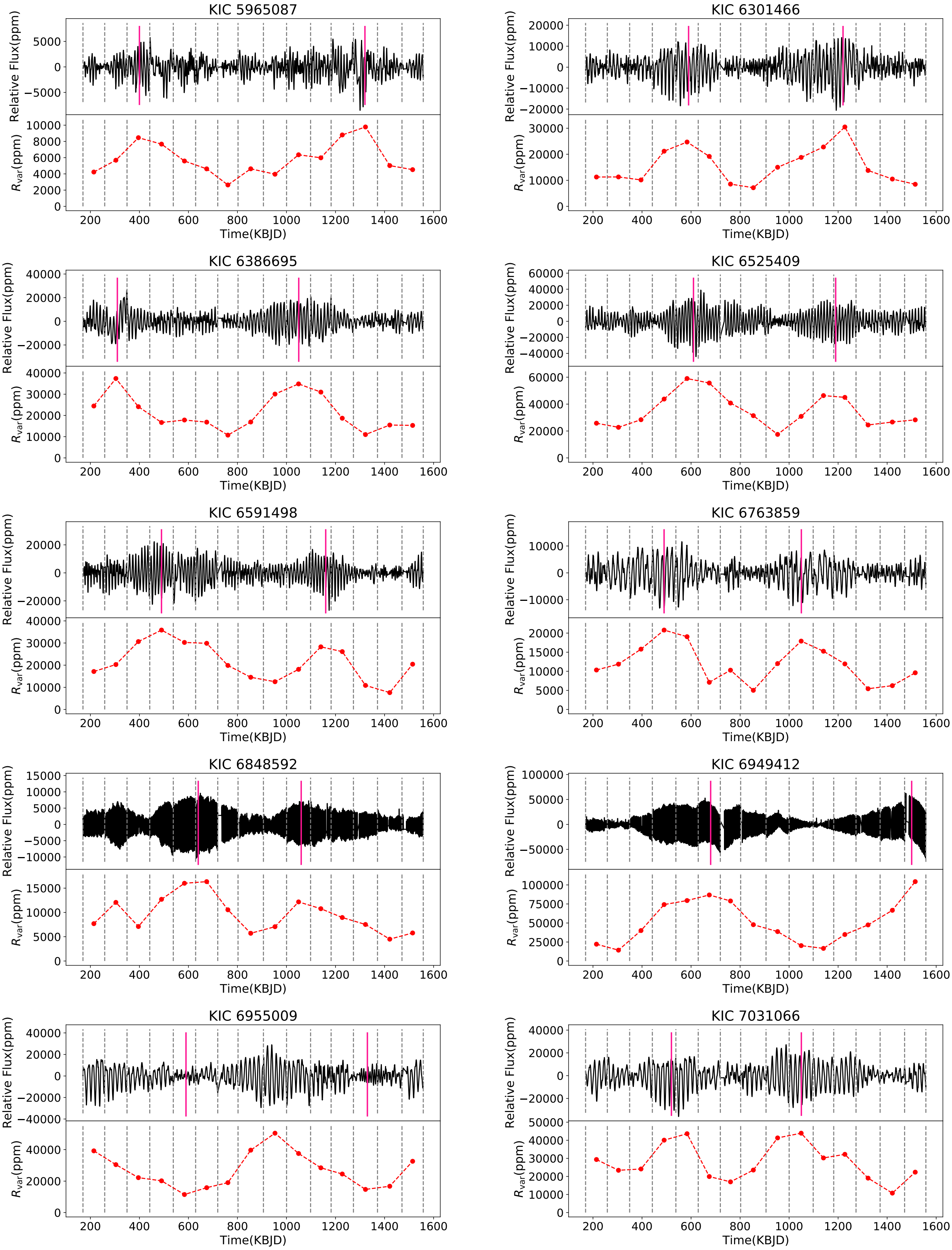

Research and Development Program of China (NKRDPC, Grant Nos. 2016YFA0400804, 2019YFA0405000 and 2019YFA0405504).

References

Babcock, H. W. 1953, ApJ, 118, 387
Babcock, H. W., & Babcock, H. D. 1955, ApJ, 121, 349

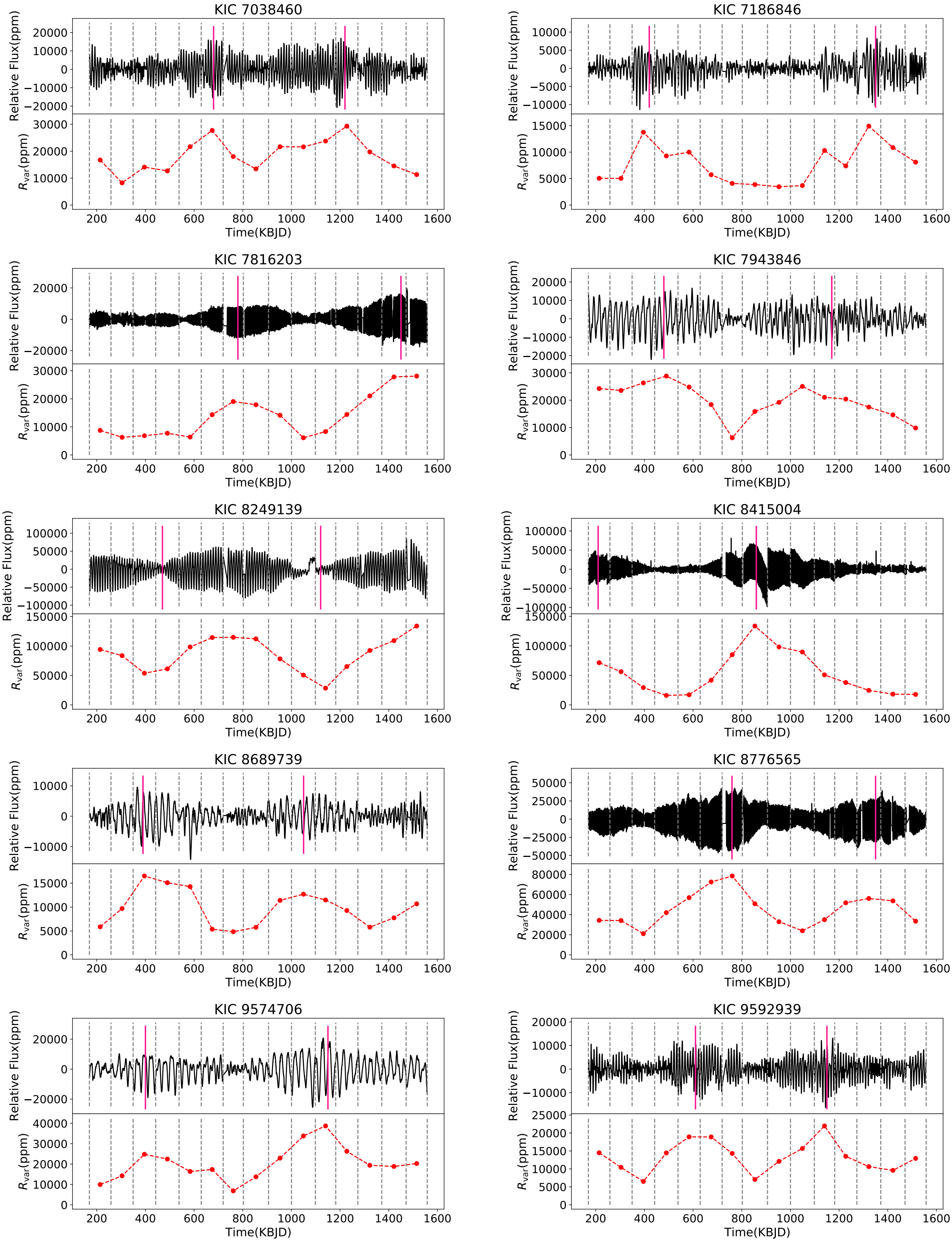

Balona, L. A. 2013, MNRAS, 431, 2240
Basri, G., Walkowicz, L. M., Batalha, N., et al. 2011, AJ, 141, 20
Basri, G. 2018, ApJ, 865, 142
Basri, G., & Shah, R. 2020, ApJ, 901, 14
Böhm-Vitense, E. 2007, ApJ, 657, 486
Boro Saikia, S., Marvin, C. J., Jeffers, S. V., et al. 2018, A&A, 616, A108
Brandenburg, A., Saar, S. H., & Turpin, C. R. 1998, ApJL, 498,

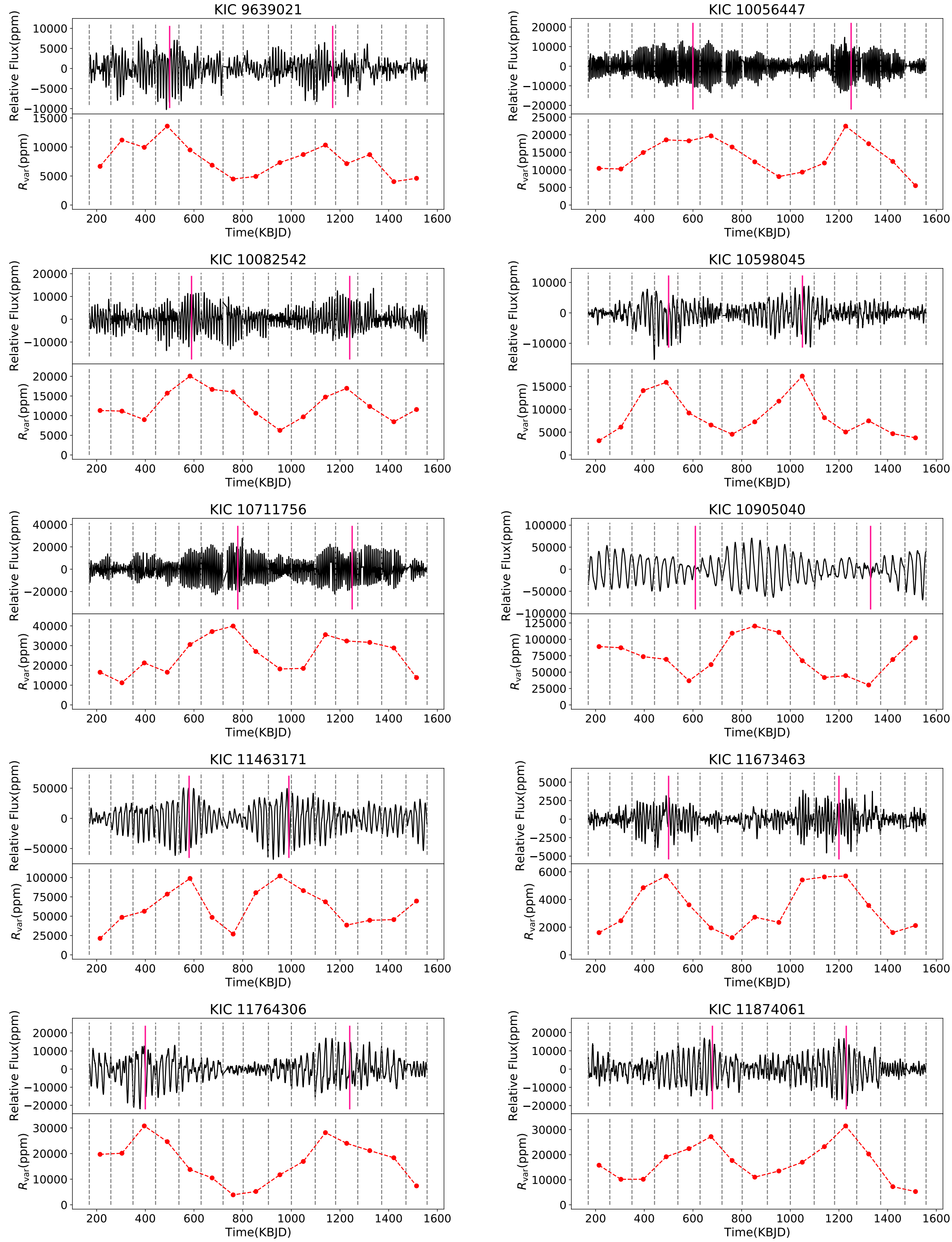

L51

Breger, M. 1979, PASP, 91, 5

Brown, T. M., Latham, D. W., Everett, M. E., & Esquerdo, G. A. 2011, AJ, 142, 112

Charbonneau, P. 2010, Living Reviews in Solar Physics, 7, 3

Cui, K., Liu, J., Yang, S., et al. 2019, MNRAS, 489, 5513

Distefano, E., Lanzafame, A. C., Lanza, A. F., et al. 2017, A&A, 606, A58

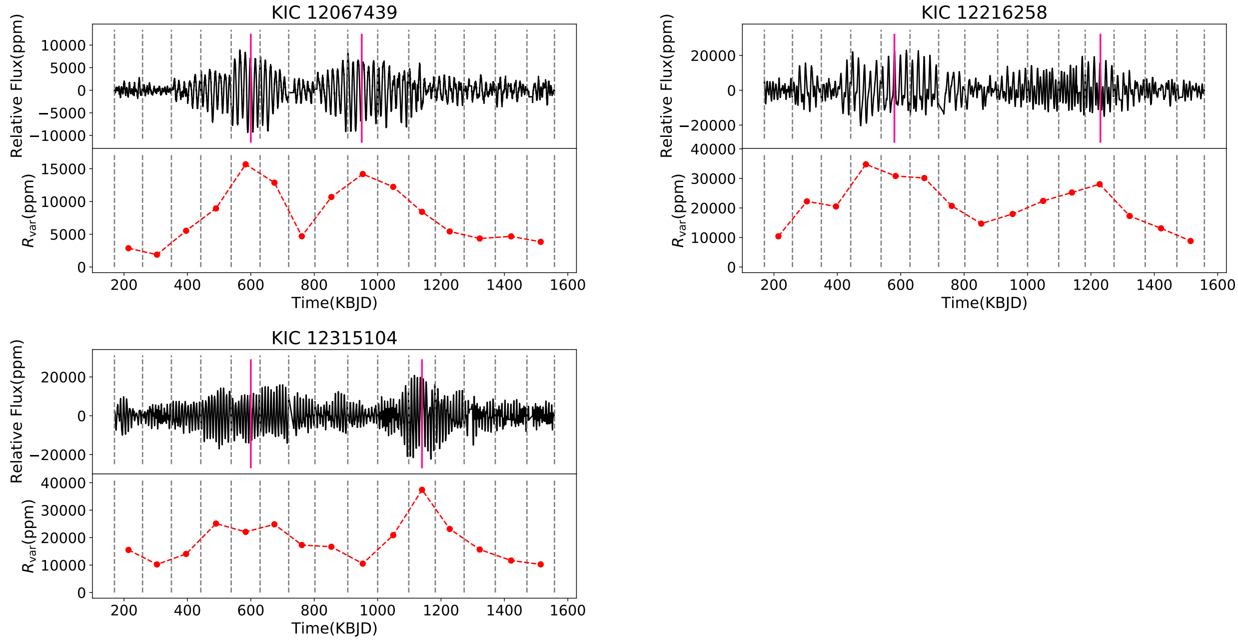

Dziembowski, W. A., Moskalik, P., & Pamyatnykh, A. A. 1993, MNRAS, 265, 588
Egeland, R., Metcalfe, T. S., Hall, J. C., & Henry, G. W. 2015, ApJ, 812, 12
Egeland, R., Soon, W., Baliunas, S., et al. 2017, ApJ, 835, 25
Ferreira Lopes, C. E., Leão, I. C., de Freitas, D. B., et al. 2015, A&A, 583, A134
Fröhlich, C., & Lean, J. 1998, Geophys. Res. Lett., 25, 4377
Hall, J. C., Henry, G. W., & Lockwood, G. W. 2007, AJ, 133, 2206
Harvey, K. L. 1992, in Astronomical Society of the Pacific Conference Series, 27, The Solar Cycle, ed. K. L. Harvey, 335
Kaye, A. B., Handler, G., Krisciunas, K., et al. 1999, PASP, 111, 840
Koch, D. G., Borucki, W. J., Basri, G., et al. 2010, ApJL, 713, L79
Leighton, R. B. 1959, ApJ, 130, 366
Lomb, N. R. 1976, Ap&SS, 39, 447
Maehara, H., Notsu, Y., Notsu, S., et al. 2017, PASJ, 69, 41
Mathur, S., García, R. A., Ballot, J., et al. 2014, A&A, 562, A124
McQuillan, A., Mazeh, T., & Aigrain, S. 2014, ApJS, 211, 24
Metcalfe, T. S., Buccino, A. P., Brown, B. P., et al. 2013, ApJL, 763, L26
Metcalfe, T. S., Egeland, R., & van Saders, J. 2016, ApJL, 826, L2
Metcalfe, T. S., Basu, S., Henry, T. J., et al. 2010, ApJL, 723, L213
Montet, B. T., Tovar, G., & Foreman-Mackey, D. 2017, ApJ, 851, 116
Noyes, R. W., Hartmann, L. W., Baliunas, S. L., et al. 1984, ApJ, 279, 763
Oláh, K., Kolláth, Z., Granzer, T., et al. 2009, A&A, 501, 703
Olspert, N., Lehtinen, J. J., Käpylä, M. J., et al. 2018, A&A, 619, A6
Parker, E. N. 1955a, ApJ, 122, 293
Parker, E. N. 1955b, ApJ, 121, 491
Preminger, D. G., Chapman, G. A., & Cookson, A. M. 2011, ApJL, 739, L45
Radick, R. R., Lockwood, G. W., Skiff, B. A., & Baliunas, S. L. 1998, ApJS, 118, 239
Reinhold, T., Bell, K. J., Kuszlewicz, J., et al. 2019, A&A, 621, A21
Reinhold, T., Cameron, R. H., & Gizon, L. 2017, A&A, 603, A52
Reinhold, T., Shapiro, A. I., Solanki, S. K., et al. 2020, Science, 368, 518
Saar, S. H., & Brandenburg, A. 1999, ApJ, 524, 295
Salabert, D., García, R. A., Jiménez, A., et al. 2017, A&A, 608, A87
Scargle, J. D. 1982, ApJ, 263, 835
Schwabe, M. 1843, Astronomische Nachrichten, 20, 283
Shapiro, A. I., Solanki, S. K., Krivova, N. A., et al. 2016, A&A, 589, A46
Shapiro, A. I., Solanki, S. K., Krivova, N. A., et al. 2017, Nature Astronomy, 1, 612
Solanki, S. K., Inhester, B., & Schüssler, M. 2006, Reports on Progress in Physics, 69, 563
Solanki, S. K., Krivova, N. A., & Haigh, J. D. 2013, ARA&A, 51, 311
Stumpe, M. C., Smith, J. C., Van Cleve, J. E., et al. 2012, PASP, 124, 985
Van Cleve, J. E., & Caldwell, D. A. 2016, Kepler Instrument Handbook, Tech. rep., Kepler Science Document, KSCI-19033-002
Vida, K., Oláh, K., & Szabó, R. 2014, MNRAS, 441, 2744
Wilson, O. C. 1978, ApJ, 226, 379
Wright, N. J., Drake, J. J., Mamajek, E. E., & Henry, G. W. 2011, ApJ, 743, 48
Yang, H., Liu, J., Gao, Q., et al. 2017, ApJ, 849, 36
Yang, H., & Liu, J. 2019, ApJS, 241, 29
Yeo, K. L., Krivova, N. A., Solanki, S. K., & Glassmeier, K. H. 2014, A&A, 570, A85